ACS APPLIED MATERIALS & INTERFACES

Research Article

www.acsami.org

Combining Top-Down and Bottom-Up Routes for Fabrication of Mesoporous Titania Films Containing Ceria Nanoparticles for Free Radical Scavenging

Alessandra Pinna,[†] Barbara Lasio,[†] Massimo Piccinini,[†] Benedetta Marmiroli,[‡] Heinz Amenitsch,[‡] Paolo Falcaro,[§] Yasuaki Tokudome,[∥] Luca Malfatti,[†] and Plinio Innocenzi*[,†]

[†]Laboratorio di Scienza dei Materiali e Nanotecnologie, LMNT-D.A.D.U., Università di Sassari and CR-INSTM, Palazzo Pou Salit, Piazza Duomo 6, 07041 Alghero, Sassari, Italy

[‡]Institute of Inorganic Chemistry, Graz University of Technology, Stremayrgasse 9/IV 8010 Graz, Austria

[§]Division of Materials Science and Engineering, CSIRO, Private Bag 33, Clayton South MDC 3169, Australia

[∥]Department of Materials Science, Graduate School of Engineering, Osaka Prefecture University, Sakai, Osaka 599-8531, Japan

ABSTRACT: Nanocomposite thin films formed by mesoporous titania layers loaded with ceria nanoparticles have been obtained by combining bottom-up self-assembly synthesis of a titania matrix with top-down hard X-ray lithography of nanocrystalline cerium oxide. At first the titania mesopores have been impregnated with the ceria precursor solution and then exposed to hard X-rays, which triggered the formation of crystalline cerium oxides within the pores inducing the in situ growth of nanoparticles with average size of 4 nm. It has been observed that the type of coordinating agent in the solution plays a primary role in the formation of nanoparticles. Different patterns have been also produced through deep X-ray lithography by spatially controlling the nanoparticle growth on the micrometer scale. The radical scavenging role of the nanocomposite films has been tested using as a benchmark the UV photodegradation of rhodamine 6G. After impregnation with a rhodamine 6G solution, samples with and without ceria have shown a remarkably different response upon exposure to UV light. The dye photodegradation on the surface of nanocomposite films appears strongly slowed down because of the antioxidation effect of ceria nanoparticles.

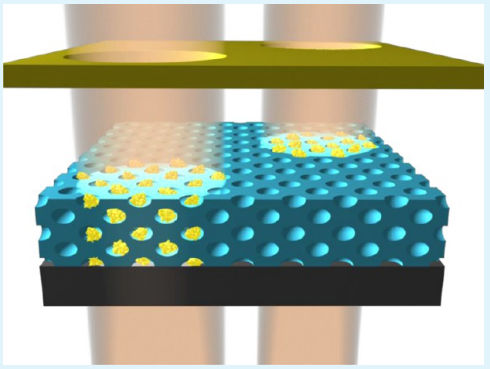

KEYWORDS: *cerium oxide, nanoparticles, mesoporous film, lithography*

INTRODUCTION

The integration of bottom-up and top-down routes has recently become one of the main challenges for fabricating nanodevices with advanced functional properties. In particular, it has been shown that high-energy X-rays allow for direct patterning of soft matter and fabrication of devices by a fast and extremely versatile protocol.[1] The combination of hard X-ray and soft matter has several advantages; in fact, when a material is still in its "soft" state, it can be directly modified and patterned by hard X-rays. Sol−gel,[2,3] hybrid organic−inorganic materials,[4] mesoporous films,[5] metal−organic frameworks (MOFs),[6] and block copolymers[7] have shown to be suitable for integrating bottom-up and top-down fabrications. The combination of the two methods turned out to be particularly effective when applied to functional mesoporous films; in fact, a mesoporous ordered film can be obtained via self-assembly through organization of supramolecular templates and the film lithography performed immediately after deposition allows for the densification of the wall structure and removal of the surfactant in one single step. Furthermore, when nanoparticle precursors are added to the material by one-pot synthesis or post impregnation of preformed films, X-ray exposure can be exploited to promote the growth of metal nanoparticles (NPs), such as gold[8] and silver,[9] within the porous matrix. The nanoparticles nucleate and grow in the film regions exposed to the X-ray beam, and this represents therefore a direct lithographic method for writing the material and producing devices for different applications such as nanoelectrodes[10] and surface-enhanced Raman spectroscopy (SERS) layers.[6]

The functionalization of the porous matrix with oxide NPs would also be very interesting, but up to now, the achievement of a spatial control required for patterning a mesoporous film by controlled nucleation and growth of nano-objects is still a difficult task. In particular, crystalline cerium oxide (ceria) nanoparticles are of paramount importance because of their catalytic and radical scavenging properties.[11,12] The functional properties of ceria nanoparticles are related to the large number of surface defects, primarily oxygen vacancies, that allow switching the cerium oxidation state between III and IV.[13] This autocatalytic process plays a role comparable to the antioxidant

Received: January 9, 2013
Accepted: March 13, 2013
Published: March 13, 2013

species present in biological systems such as the super oxide dismutase.[14] The controlled formation of nanoparticles into a porous matrix would open the route to several important applications, especially in the field of nanobiotechnology.[15] In fact, the design of smart nanocomposite surfaces could be applied for the fabrication of cell chambers and/or dishes for cell culture. The incorporation of functional properties at the interface between chambers and cells offers several advantages such as, for instance, a close interaction between biological species and the nanocomposite surface with no need of dispersing/capping agents or pH buffers to avoid particle aggregation in the cell media.

In the present work we have developed a combination of bottom-up and top-down processing, which allows producing ceria nanoparticles of controlled dimensions within a mesoporous ordered titania film. The overall material fabrication has been optimized to minimize the crystallization of the titania matrix allowing at the same time the writing of selected areas with ceria nanoparticles having radical scavenging properties.

EXPERIMENTAL SECTION

Cerium(III) nitrate hexahydrate ($Ce(NO_3)_3{\cdot}6H_2O$, ABCR 99.9%), urea (CH_4N_2O, Aldrich 99%), 1-hexadecyl-trimethylammonium bromide (CTAB, ABCR 98%), Pluronic F127 (PEO_{106}-PPO_{70}-PEO_{106}, Aldrich), 2-propanol (Carlo Erba 99.7%,), 1 M hydrochloric acid (HCl, Aldrich), titanium tetrachloride ($TiCl_4$, Aldrich), ethanol (EtOH, Fluka 99.8%), and rhodamine 6G (Rh6G, Aldrich) were used as received without further purification; bidistilled water (H_2O) was employed in the synthesis. Silicon wafers, p-type boron-doped, and silica glass slides were employed as substrates for film deposition.

Synthesis of the Precursor Sols. Titania sol was prepared using $TiCl_4$, EtOH, H_2O, and Pluronic F127, with the following molar ratios: $TiCl_4$:EtOH:F127:H_2O = 1:40:0.005:10. The precursor sol was obtained by addition of $TiCl_4$ into a mixture of EtOH and surfactant Pluronic F127 after 5 min of stirring; water was then added dropwise at the precursor sol. Titania sol was deposited by dip-coating in a controlled chamber, with 25% relative humidity (RH) and a withdrawal rate of 15 cm·min^{-1}. After deposition, the films were dried in an oven at 60 and 130 °C (24 h at each temperature). The samples were then calcined thermally treating them from 130 °C up to 350 °C with a heating rate of 1 °C min^{-1}, with a final firing step of 2 h at 350 °C.

The ceria precursor sol was prepared by dissolving 2 g of urea, CTAB, or Pluronic F127 and 0.5 cm^3 of HCl in 20 cm^3 of 2-propanol and left under stirring for 5 min; this solution was then added dropwise to the cerium nitrate solution which was previously prepared by dissolving 7 g of $Ce(NO_3)_3{\cdot}6H_2O$ and 0.5 cm^3 of HCl in 20 cm^3 of 2-propanol. The precursor sol was then deposited by spin coating on a titania mesoporous film using 400 rpm for 40 s.

The as-prepared films were directly exposed to hard X-ray radiation using the deep X-ray lithography (DXRL) beamline at Elettra synchrotron facility (Trieste, Italy). The storage ring worked at 2 GeV. The sample was mounted on top of a water-cooled stainless steel plate (scanner), which was continuously rastering the sample in front of the beam to allow for a homogeneous exposure of areas larger than the beam size; the scanner rate was set to 20 mm s^{-1}. At the exposure plane (position of the sample) the beam size was 115.5 mm × 10.6 mm. The films were irradiated with different doses (energy per unit area at the sample surface) by changing the exposure time (61, 132, and 234 s). In fact, the energy per unit area is equal to the exposure time multiplied by the X-ray power per unit area, hitting the sample P = 2.472 W cm^{-2}. The films were exposed to doses corresponding to 163, 326, and 653 J cm^{-2}. A mask containing test patterns of different size, shape, and geometry (5−500 μm) was then used to produce patterns on the films that were exposed to the X-ray beam. The mask had a gold absorber 20 μm thick and a titanium transparent membrane with thickness of 2.2 μm.

Mesoporous titania films were exposed, without mask, to the same X-ray doses of the patterned samples and then impregnated with a solution containing ethanol and Rh6G (5×10^{-3} M) to test the antioxidant properties. Afterward, the films were placed at a distance of around 5 mm from a UV lamp and exposed to UV radiations for increasing time. The lamp mounted a fluorescence tube for emission at λ = 365 nm with a nominal power density of 470 μW cm^{-2} at 15 cm. As a reference, Rh6G was deposited on silica slides and on pure titania films, not containing ceria nanoparticles and not exposed to DXRL; the samples were then exposed to UV light following the above protocol.

Materials Characterization. X-ray diffraction (XRD) patterns of titania mesoporous films, loaded with CeO_2 nanoparticles, were collected using a Bruker D8 Discover diffractometer in grazing incidence geometry using a Cu K_α line (λ = 1.54056 Å); the X-ray generator worked at a power of 40 kV and 40 mA. The patterns were recorded in 2θ ranging from 10 to 100° with a step size of 0.02° and a scan speed of 0.5 s by a repetition mode for 12 h until maximization of the signal-to-noise ratio. The XRD data were analyzed with the MAUD software[16] according to the Rietveld method.[17]

TEM images were taken with a transmission electron microscope (TEM; JEM-2000FX, JEOL, Japan) operating at voltage of 200 kV. For observation, the films were scratched into fine powders and then dispersed in ethanol to form a slightly turbid suspension. A small drop of the resultant suspension was placed on a carbon-coated copper mesh grid and dried at room temperature. Pore and ceria nanoparticle sizes were estimated from line profile analysis performed on representative TEM images with the ImageJ program.[18]

A Wollam-α spectroscopic ellipsometer with fixed angle geometry was used for thickness measurements of thin films deposited on silicon substrates. The thickness was estimated by fitting the experimental data with a Cauchy model for transparent films on Si substrates. The fit showed an average mean square error (MSE) of about 12 for titania mesoporous films and 20 for titania mesoporous films loaded with ceria nanoparticles.

The mesostructure characterization of the titania films was performed using synchrotron radiation by small-angle X-ray scattering (SAXS) in grazing incidence (GISAXS) mode at the Austrian high-flux beamline of the electron storage ring ELETTRA (Trieste, Italy). The angle of incidence of the beam (λ = 1.54 Å) was set either to 90° (transmission mode) or slightly above the critical angle (grazing incidence mode or GISAXS). Two-dimensional patterns were recorded with a CCD detector (Photonic Science).

A Raman microscope was used to detect the formation of ceria nanoparticles inside the titania mesoporous films. A Bruker Senterra confocal Raman microscope working with a laser excitation wavelength of 532 nm at 12 mW of nominal power was used for optical microscopy (100× magnification) and Raman spectroscopy analysis; the spectra were recorded by averaging 30 acquisitions of 2 s. Raman imaging maps were obtained by selecting the 100× objective, and an array of 10 × 10 points was defined to cover an area of 35 × 35 μm with a step of 3.5 μm. Each spectrum of the map was recorded by averaging five acquisitions of 5 s.

A Bruker M4 Tornado X-ray fluorescence spectrometer with a 10× objective was used to observe the Ce and Ti element content over an area of 1.8 × 1.8 mm of titania mesoporous films patterned with ceria nanoparticles. The samples were washed with fresh 2-propanol before measuring, to remove the unreacted ceria precursors from the unexposed regions. The maps were recorded under vacuum using an X-ray tube with Rh anode at 600 μA and 50 KV without any filter and with a spot size of 4 μm.

Absorption spectra of the Rh6G deposited on bare silica slides and CeNPs-loaded mesoporous titania films were measured in the 200−900 nm wavelength range using a UV−vis Nicolet Evolution 300 spectrometer, at 500 nm·min^{-1} scan rate. Each acquisition was the average of three different scans collected with a bandwidth of 1.5 nm.

RESULTS AND DISCUSSION

The synthesis of titania mesoporous ordered films is based on self-assembly of a pore templating agent triggered by solvent evaporation; this is a well-established route, and several types of ordered titania films can be obtained using a variety of surfactants.[19] In the first step of the present synthesis we have prepared mesoporous ordered titania films by employing a triblock copolymer, Pluronic F127, as a template; the films result well ordered even after the thermal treatment at 350 °C used to remove the template.[20] The firing temperature has been selected to optimize the film properties; in fact, after thermal processing the organic template is fully removed, and the mesoporous titania films maintain the mesostructure.[21]

Figure 1 shows the GISAXS pattern of a titania mesoporous film after thermal treatment at 130 °C for 24 h and 350 °C for another 2 h; the pattern is characteristic of an $Im\bar{3}m$ in the space group contracted along the [110] direction. The GISAXS pattern confirms that the mesostructure is retained after processing and the thermally induced uniaxial shrinkage[22] produces a small distortion of the pore structure.

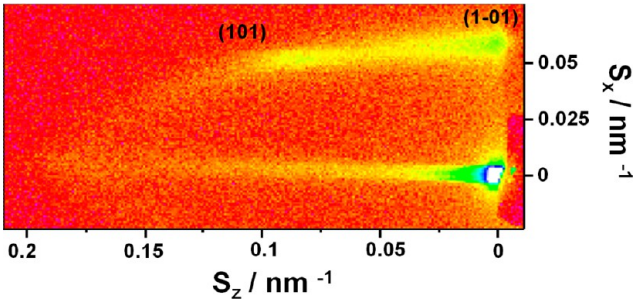

Figure 1. GISAXS pattern of a titania mesoporous film after thermal treatment at 130 °C for 24 h and 350 °C for another 2 h; the pattern is characteristic of an $Im\bar{3}m$ in the space group mesostructure contracted along the [110] direction.

In the second step of the preparation, the titania-ordered mesoporous films were impregnated with the ceria precursor solution via spin coating that has shown to be the most effective route, while other methods (e.g., casting) have not given a homogeneous pore filling.

The samples have been exposed to hard X-rays, generated by a synchrotron source, to induce the formation of ceria nanoparticles within the pores; the overall process is shown in Figure 2. The photons that have been used to irradiate the samples have energy between 2500 and 12 000 eV[3], and they have been used in previous works as a lithographic tool for soft matter and in situ formation of metal nanoparticles in mesoporous films. As expected, the exposure to hard X-rays has induced the formation of ceria nanoparticles with selective control of the areas where these CeNPs grew up. Compared to other techniques, such as UV photoassisted ceria synthesis,[23,24] a major advantage of the deep X-ray lithography is the penetration depth that can be reached;[25] this allows forming nanoparticles throughout the whole film thickness. Another advantage of DXRL is the loading that can be obtained; the authors have already tried to impregnate a mesoporous film with nanoparticles by using alternative approaches, such as post impregnation with colloidal nanoparticle solution or in situ formation of ceria nanoparticles. To the best of our knowledge, however, these techniques do not allow a homogeneous loading of the inner part of the porous films.

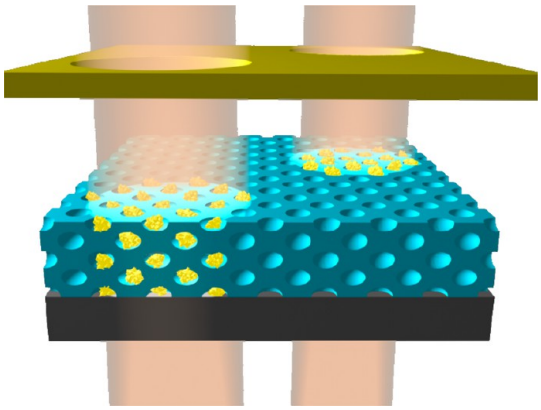

Figure 2. Drawing of the patterning process by in situ nucleation and growth of ceria nanoparticles.

The mesoporous films have been therefore exposed to increasing doses of radiation, and the effect has been evaluated by electron microscopy, XRD, and Raman spectroscopy.

TEM images of Figure 3 show representative bright (a) and dark (b) field images of the mesoporous film after X-ray exposure at the highest dose (653 J cm^{-2}). The samples retain the typical morphology of ordered porous films where pores in the mesoscale are stacked in a close cubic fashion. We have used a plot profile analysis of a large set of measurements to evaluate an average pore size of 5.4 ± 0.6 nm. This value, within the experimental error, is consistent with previous findings that also measured the surface area of the titania porous sample fired at 350 °C.[26] Following this reference, therefore, we have assumed a film surface of roughly 595 m^2·cm^3. The dense and homogeneous distribution of the nanoparticles inside the porous matrix is clearly shown in the dark field images where the white spots are due to the cerium oxide nanocrystals; the average size of the nanoparticles has been estimated as 3.8 ± 0.9 nm.

Spectroscopic ellipsometry has been used as a tool to evaluate differences in the film thickness before the X-ray exposure at 653 J cm^{-2}. The average thickness of all the samples is around 180 ± 20 nm, and we do not observe shrinkage after X-ray-induced nanoparticle formation.

Figure 4 shows the XRD patterns in the angular range 20–100° of calcined titania mesoporous film whose pores have been filled with the urea–Ce solution (green line) and after exposure to 163 J cm^{-2} (black line), 326 J cm^{-2} (red line), and 653 J cm^{-2} (blue line) doses. After exposure to the lowest dose, the detection of a pattern with different sharp diffraction peaks indicates very likely the fragmentation of the cerium nitrate induced by radiations. These peaks decrease in intensity and partially disappear after exposure to a higher dose, 326 J cm^{-2}, and are not detected any longer in the samples exposed to the highest radiation dose, 653 J cm^{-2}. On the other hand, with the increase of the dose, the films exhibit a diffraction pattern characterized by several broad and intense peaks which can be unambiguously assigned to crystalline cerium oxide. The diffraction peaks correspond to the (111), (200), (220), (311), (400), (331), (420), (422), and (511) planes of the cubic fluorite structure of CeO_2 cerianite.[27] It is also important to note that the thermal treatment at 350 °C and the exposure to X-rays do not induce further crystallization of titania, which is so little that it could not be detected by XRD. This point is particularly interesting because nanocrystallites of anatase

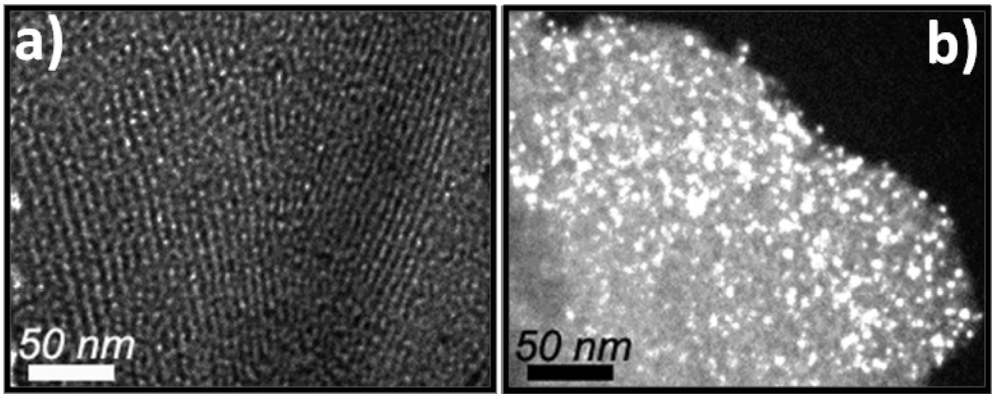

Figure 3. TEM images of (a) titania mesoporous film (bright field) and (b) titania mesoporous film with ceria nanoparticles (dark field) after X-ray exposure at the highest dose (653 J cm^{-2}).

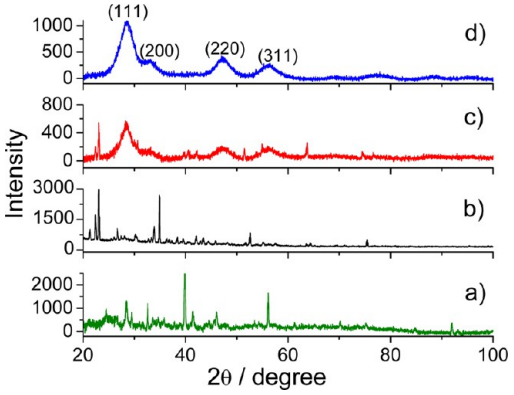

Figure 4. XRD patterns of titania mesoporous films at different processing steps: (a) as-prepared mesoporous titania film after filling the pores with urea–ceria solution (green line); (b) after exposure to a dose of 163 J cm^{-2} (black line); (c) after exposure to a dose of 326 J cm^{-2} (red line), and (d) after exposure to a dose of 653 J cm^{-2} (blue line).

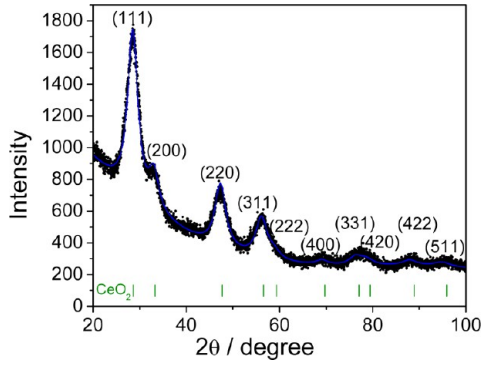

Figure 5. XRD pattern (black dots) of ceria nanoparticles after hard X-ray exposure (653 J cm^{-2}). The Rietveld fit is reported as a continuous blue line.

titania promote the formation of free radicals, while nanoparticles of ceria have the property of acting as a radical scavenger. The two effects could compete if titania crystallizes; nonetheless, in the present case, we have managed to find a method that allows producing nanocrystalline ceria within a solid mesoporous framework with a minimum amount of crystallinity. On the other hand, mesoporous titania has the advantage to be highly hydrolytically stable in comparison to silica-based mesoporous materials and is more suitable to develop applications when chemical durability in water environment is requested.[28]

We have characterized the ceria nanoparticles from XRD patterns using the Rietveld method; the fit (Figure 5) gives 4.05 nm for the crystallite size and 0.545 nm for lattice parameter *a*, which is the same value reported for CeO_2 in the standard data (a = 0.541 nm, space group $Fm3m$),[16] and the microstrain is 0.0029. At the highest exposure dose the films result in being composed of mesoporous titania whose pores contain a ceria nanoparticle with an average dimension of 4 nm, in accordance with TEM analysis.

Raman spectroscopy has been performed on the irradiated samples to detect the formation of cerium oxide; in detail, it has followed the evolution of the 465 cm^{-1} Raman active mode of cerium oxide, which is due to the symmetric breathing vibrations of the oxygen anions around the cerium cation.[29]

Figure 6 shows the Raman spectra in the 480–100 cm^{-1} range of urea–Ce titania mesoporous films upon exposure to

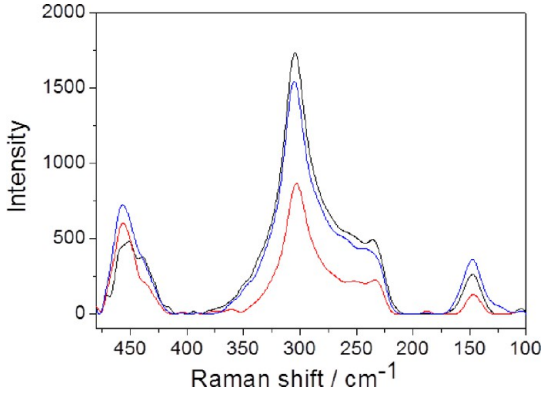

Figure 6. Raman spectra in the 475–410 cm^{-1} range of mesoporous films whose pores have been filled by cerium nitrate and urea solution after exposure to a dose of 163 J cm^{-2} (black line), 326 J cm^{-2} (red line), and 653 J cm^{-2} (blue line).

different doses: 163 J cm^{-2} (black line), 326 J cm^{-2} (red line), and 653 J cm^{-2} (blue line). The Raman mode of ceria is clearly observed in the samples exposed to 326 and 653 J cm^{-2}, while around 143 and 450 cm^{-1}, there are two bands which are attributed to anatase and rutile phases, which are formed in the mesoporous structure as a consequence of the thermal treatment.[30] The crystalline fraction of the films and the size

dx.doi.org/10.1021/am4001024 | ACS Appl. Mater. Interfaces 2013, 5, 3168–3175

of the crystalline domains, however, are very small since the XRD patterns (vide infra) do not show diffraction peaks attributed to titania phases.

We have also tested two other precursor solutions of ceria, which have been used to impregnate the mesopores of titania films through an identical protocol. Figures 7 and 8 show the

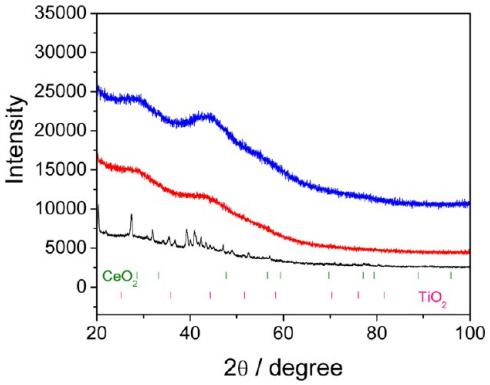

Figure 7. XRD patterns of titania mesoporous films whose pores have been filled by using a cerium nitrate and Pluronic F127 solution after exposure to a dose of 163 J cm^{-2} (black line), 326 J cm^{-2} (red line), and 653 J cm^{-2} (blue line).

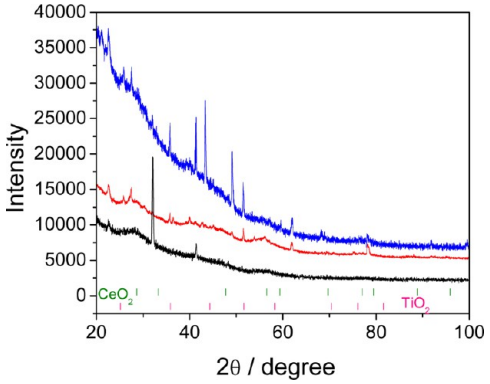

Figure 8. XRD patterns of titania mesoporous films whose pores have been filled by using a cerium nitrate and CTAB solution after exposure to a dose of 163 J cm^{-2} (black line), 326 J cm^{-2} (red line), and 653 J cm^{-2} (blue line).

XRD patterns of the mesoporous films whose pores have been impregnated by a precursor solution containing cerium nitrate and, respectively, Pluronic F127 and CTAB. After impregnation, similarly to the urea−ceria samples, the films have been exposed to increasing doses of hard X-rays.

The comparison among the different preparation methods shows that the results are considerably different and the type of surfactant appears therefore to play a fundamental role in the formation of ceria nanoparticles upon exposure to hard X-rays. In the case of Pluronic-F127 samples (Figure 7), ceria nanoparticles are formed, but the XRD peaks attributed to cerium oxide are less intense and wider, indicating the formation of nanoparticles with smaller dimension. In the case of sample prepared with CTAB as surfactant, only a very weak and wide signal assigned to ceria could be observed (Figure 8), indicating that CTAB does not allow an efficient formation of ceria nanoparticles. The sharp peaks are assigned to fragmentation of precipitates from the precursor sol produced by the X-ray exposure.

A comparison of the different results obtained employing a block copolymer (Pluronic F127), an ionic surfactant (CTAB), and a coordinating agent (urea) gives some indications about the formation of the ceria nanoparticles by DXRL. We have seen that the dose plays an important role; only when some threshold value is reached, the ceria nanoparticles form. The first effect is the fragmentation of the compounds that crystallize after solvent evaporation of the precursor solution inside the mesoporous films. The second one is the production of free radicals $OH^{\bullet}$ that induce the oxidation of Ce^{3+} to Ce^{4+}. The overall effect, however, depends on the dispersing/coordinating agent that has been used in the solution of ceria precursors to impregnate the films; in fact the formation of ceria nanoparticles is effective with urea and, to some extent, with Pluronic but does not work with CTAB. The amines in urea play, most likely, a primary role by favoring the nucleation process of ceria nanocrystals via coordination of Ce^{4+} ions,[31] and a similar mechanism should be activated in the presence of triblock copolymers. On the other hand the CTAB, characterized by a cationic moiety, is not able to coordinate the Ce^{4+} because of the charge repulsion that disfavors the nucleation process.

Ceria nanoparticles are of paramount importance because of their catalytic and radical scavenging properties, and the controlled formation into a porous matrix should enable the fabrication of antioxidant substrates for cell cultures. We have performed a simple test to verify the antioxidant effect by measuring the photodegradation of a dye, Rh6G, when deposited on a silica slide, bare mesoporous titania films, or mesoporous titania films loaded with ceria nanoparticles. The three samples have been then exposed to UV light at 365 nm monitoring the photodegradation of Rh6G as a function of time by UV−visible spectroscopy (Figure 9a, b, and c respectively). Before exposure, the absorption spectrum of the films in the 400−600 nm range is mainly due to the typical absorption bands of Rh6G in the form of monomers and dimers. Rh6G dimers, in fact, have two distinct absorption maxima, at higher (*J*-type dimers) and lower (*H*-type dimers) wavelengths with respect to the absorption peak of the monomer band (≈530 nm).[32] After 1 h of exposure, the decrease of absorbance percentage, in the films without NPs, is higher compared to pure Rh6G on silica, indicating a weak photocatalytic effect of the porous matrix. On the contrary, the absorbance of the film loaded with ceria NPs shows a slower and less sharp decrease if compared to the photodegradation of the pure dye on silica. Figure 9d shows the value of the integrated absorbance in the range between 400 and 600 nm as a function of the UV exposure time. The bleaching effect due to Rh6G photodegradation is clearly visible both in the dye on silica and in the film without NPs, where the absorbance decreases roughly 70% after 5 h of exposure. The degradation of the dye not deposited on mesoporous films may be considered somehow surprising since it should not absorb the UV light in the 365 nm range.[33] However, this effect is easily explained if we consider that the UV lamp is not completely monochromatic and the photodegradation can be triggered by the formation of radical species from the residual solvent among the dye molecules or by the environmental moisture (water) which can be absorbed during the exposure.

The dye degradation upon UV exposure is sensitively reduced in the films loaded with ceria, despite the weak photocatalytic effect of the substrate; after 5 h the absorbance decreases less than 50%. This effect is due to the free radical

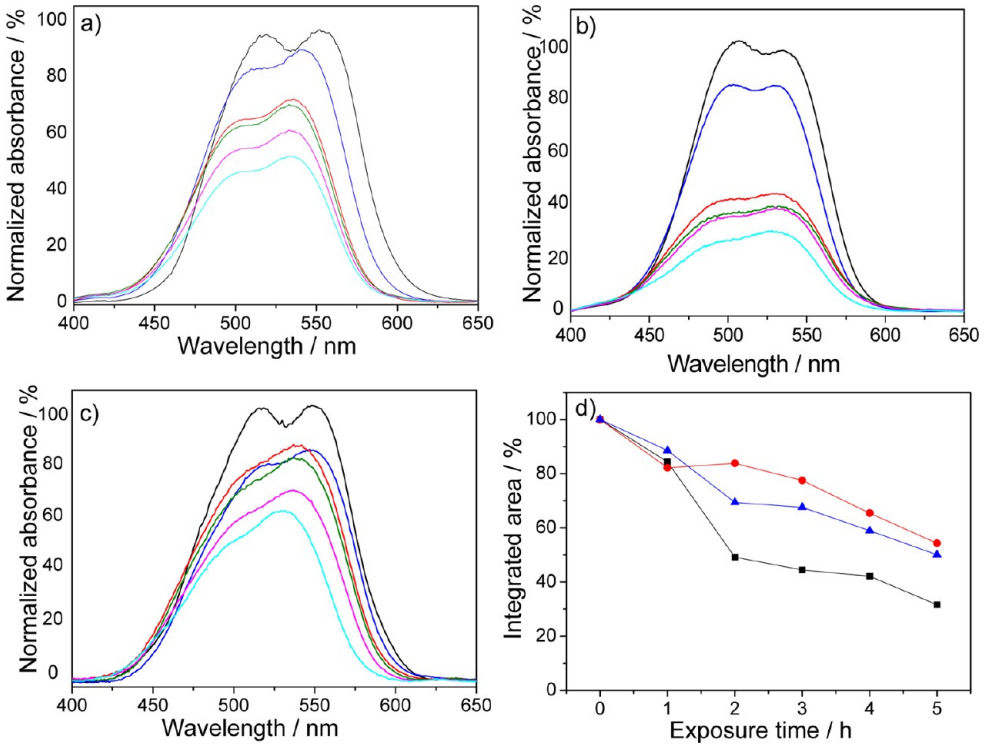

Figure 9. UV−vis absorption spectra in the 400−650 nm range of Rh6G on silica (a), Rh6G on bare mesoporous titania films (b), and NP-loaded mesoporous titania films (c) exposed to UV light for increasing times: 0 (black line), 1 h (blue line), 2 h (red line), 3 h (green line), 4 h (pink line), and 5 h (light blue line). (d) Photodegradation of Rh6G, percentage decrease of the integrated band in the 400−650 nm range as a function of the UV exposure time: the blue triangles are referred to Rh6G on silica, the black squares to Rh6G on bare film, and the red spots to Rh6G on NP-loaded film. The solid lines are guides for the eyes.

scavenging of ceria nanoparticles, which protects the organic molecules from the degradation induced by the radicals produced by UV light. According to previous results, in fact, the size of the ceria nanocrystals, grown within the porous matrix, has been tuned to maximize the radical scavenging properties of the oxide and limit its photocatalytic activity that becomes dominant for particles of larger dimensions.[34]

The antioxidant property shown by the material is of extreme interest for all those applications where it is necessary to avoid or delay the degradation of organic molecules directly induced by free radicals or indirectly caused by exposure to sources that give rise to the formation of free radicals.

The XRD and Raman data show that the exposure to high-energy photons induces the formation of ceria nanoparticles; this process has the advantage to be used for patterning the mesoporous films. DXRL, in fact, allows the controlled formation of the particles only in selected areas of the films by using proper masks; the ceria nanoparticles are formed in the part of the film which is directly exposed to the flux of photons, while in the masked side, no particles are able to grow up. Figure 10 shows the optical image of a mesoporous titania film impregnated with a urea−ceria precursor solution which has been patterned by DXRL using a dose of 653 J cm^{-2}; the areas which appear yellow have not been irradiated, while the exposed region has a dark red color. The Raman image taken on a circular spot, which represents the unexposed part where the ceria nanoparticles should not be present, is shown in Figure 11; the image is obtained by integrating the band of the Raman active mode of cerium oxide (see Figure 4), and the intensity is reported in false color scale. The area of the circular spot appears in blue, which indicates, following the intensity scale, that ceria is not present in the unexposed region.

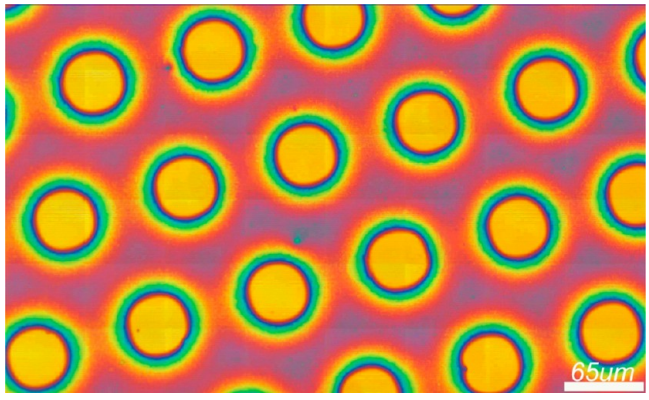

Figure 10. Optical microscope image of patterned titania mesoporous film with ceria nanoparticles. The exposure dose is 653 J cm^{-2}.

The X-ray fluorescence mapping performed on a sample, obtained by DXRL using 653 J cm^{-2} exposure dose and a urea−ceria precursor sol, gives also some interesting information as shown in Figure 12. Three different elemental maps are shown in the figure: Si (red) left side, Ti (violet) center, and Ce (yellow) right side. The Ce map well reproduces the pattern of the mask, and cerium appears to be present only in the exposed areas (the circular regions in dark correspond to the unexposed areas). Cerium partially absorbs the fluorescence from the silicon substrate, and this explains the darker color of the patterns of the silicon areas.[35] The signal of titanium is

dx.doi.org/10.1021/am4001024 | ACS Appl. Mater. Interfaces 2013, 5, 3168−3175

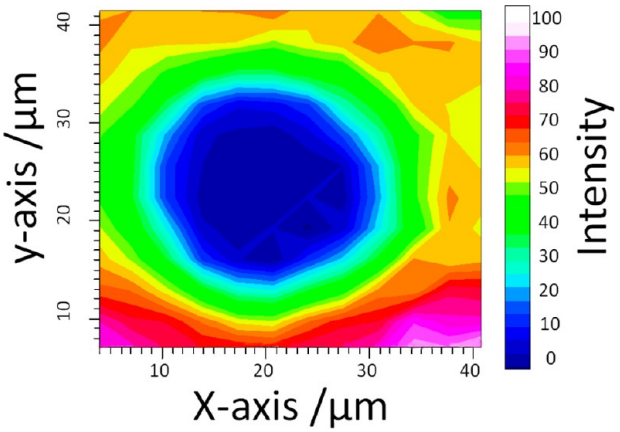

Figure 11. Raman image obtained by integrating the band of the Raman active mode of cerium oxide; the intensity is reported in false color scale. The sample has been obtained by X-ray exposure with a 653 J cm^{-2} exposure dose.

instead well homogeneously distributed, indicating the homogeneity of the sample.

CONCLUSIONS

In the present work we have successfully prepared nanocomposite films, which are formed by a mesoporous ordered titania matrix loaded with 4 nm sized nanoparticles of ceria. The particles have been nucleated and grown within the pores upon exposure to an intense source of X-rays. The formation of ceria nanoparticles induced by hard X-rays depends on the X-ray dose and the chemical nature of the compounds used to disperse the ceria precursor. It has been observed that urea is an effective agent to promote nucleation and growth of ceria, this being due to the presence of amine groups, which favor the coordination of Ce^{4+} ions.

The nanocomposite material has a radical scavenging property, as it has been demonstrated by the photodegradation experiment using Rh6G, since upon exposure to UV light the material containing the ceria nanoparticles protects the dye from photodegradation.

The top-down process allows also an easy writing of the mesoporous films; ceria nanoparticles form only in the regions exposed to X-rays, which allows for patterning the titania mesoporous films using a lithographic mask.

AUTHOR INFORMATION

Corresponding Author

*E-mail: plinio@uniss.it.

Notes

The authors declare no competing financial interest.

ACKNOWLEDGMENTS

K. Okada and N. Tarutani are gratefully acknowledged for technical support and D. Carboni and A. Soreta for helpful discussion.

REFERENCES

(1) Innocenzi, P.; Malfatti, L.; Falcaro, P. *Soft Matter* **2012**, *8*, 3722−3729.
(2) Falcaro, P.; Malfatti, L.; Vaccari, L.; Amenitsch, H.; Marmiroli, B.; Grenci, G.; Innocenzi, P. *Adv. Mater.* **2009**, *21*, 4932−4936.
(3) Innocenzi, P.; Malfatti, L.; Kidchob, T.; Costacurta, S.; Falcaro, P.; Marmiroli, B.; Cacho-Nerin, F.; Amenitsch, H. *J. Synchrotron Radiat.* **2011**, *18*, 280−286.
(4) Falcaro, P.; Costacurta, S.; Malfatti, L.; Buso, D.; Patelli, A.; Schiavuta, P.; Piccinini, M.; Grenci, G.; Marmiroli, B.; Amenitsch, H.; Innocenzi, P. *ACS Appl. Mater. Interfaces* **2011**, *3*, 245−251.
(5) Falcaro, P.; Costacurta, S.; Malfatti, L.; Takahashi, M.; Kidchob, T.; Casula, M. F.; Piccinini, M.; Marcelli, A.; Marmiroli, B.; Amenitsch, H.; Schiavuta, P.; Innocenzi, P. *Adv. Mater.* **2008**, *20*, 1864−1869.
(6) Dimitrakakis, C.; Marmiroli, B.; Amenitsch, H.; Malfatti, L.; Innocenzi, P.; Grenci, G.; Vaccari, L.; Hill, A. J.; Ladewig, B. P.; Hill, M. R.; Falcaro, P. *Chem. Commun.* **2012**, *48*, 7483−7485.
(7) Innocenzi, P.; Kidchob, T.; Costacurta, S.; Falcaro, P.; Marmiroli, B.; Cacho-Nerin, F.; Amenitsch, H. *Soft Matter* **2010**, *6*, 3172−3176.
(8) Malfatti, L.; Marongiu, D.; Costacurta, S.; Falcaro, P.; Amenitsch, H.; Marmiroli, B.; Grenci, G.; Casula, M. F.; Innocenzi, P. *Chem. Mater.* **2010**, *22*, 2132−2137.
(9) Malfatti, L.; Falcaro, P.; Marmiroli, B.; Amenitsch, H.; Piccinini, M.; Falqui, A.; Innocenzi, P. *Nanoscale* **2011**, *3*, 3760−3766.
(10) Faustini, M.; Marmiroli, B.; Malfatti, L.; Benjamin, L.; Krins, N.; Falcaro, P.; Grenci, G.; Laberty-Robert, C.; Amenitsch, H.; Innocenzi, P.; Grosso, D. *J. Mater. Chem.* **2011**, *21*, 3597−3603.
(11) Rzigalinski, B. A.; Danelisen, I.; Strawn, E. T.; Cohen, C. A.; Liang, C. *Nanoparticles for Cell Engineering − A Radical Concept*; Nanotechnologies for the Life Sciences; Wiley: New York, 2007.
(12) Karakoti, A. S.; Monteiro Riviere, N. A.; Aggarwal, R.; Davis, J. P.; Narayan, R. J.; Self, W. T.; McGinnis, J.; Seal, S. *JOM* **2008**, *60*, 33−37.
(13) Zhang, D.; Du, X.; Shia, L.; Gaoa, R. *Dalton Trans.* **2012**, *41*, 14455−14475.
(14) Korsvik, C.; Patil, S.; Sealb, S.; Self, W. T. *Chem. Commun.* **2007**, *10*, 1056−1058.

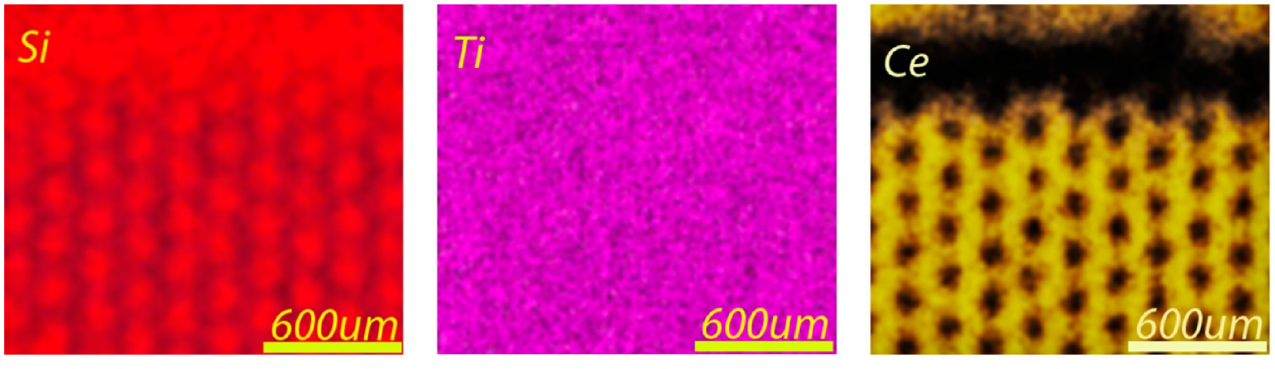

Figure 12. X-ray fluorescence map of patterned titania mesoporous film with ceria nanoparticles. Three different images are shown obtained by Si (red) left side; Ti (purple) center; and Ce (yellow) right side. The sample has been obtained by X-ray exposure with a 653 J cm^{-2} exposure dose.

(15) Pinna, A.; Figus, C.; Lasio, B.; Piccinini, M.; Malfatti, L.; Innocenzi, P. *ACS Appl. Mater. Interfaces* **2012**, *4*, 3916−3922.
(16) Lutterotti, L.; Gialanella, S. *Acta Mater.* **1998**, *46*, 101−110.
(17) Young, R. A., Ed. *The Rietveld Method*; Oxford University Press: Oxford, U.K., 1993.
(18) Schneider, C. A.; Rasband, W. S.; Eliceiri, K. W. *Nature Methods* **2012**, *9*, 671−675.
(19) Crepaldi, E. L.; Soler-Illia, G. J. A. A.; Grosso, D.; Cagnol, F.; Ribot, F.; Sanchez, C. *J. Am. Chem. Soc.* **2003**, *125*, 9770−9786.
(20) Malfatti, L.; Falcaro, P.; Amenitsch, H.; Caramori, S.; Argazzi, R.; Bignozzi, C. A.; Enzo, S.; Maggini, M.; Innocenzi, P. *Microporous Mesoporous Mater.* **2006**, *88*, 304−311.
(21) Innocenzi, P.; Malfatti, L.; Kidchob, T.; Enzo, S.; Della Ventura, G.; Schade, U.; Marcelli, A. *J. Phys. Chem. C* **2010**, *114*, 22385−22391.
(22) Innocenzi, P.; Malfatti, L.; Kidchob, T.; Falcaro, P.; Costacurta, S.; Guglielmi, M.; Mattei, G.; Bello, V.; Amenitsch, H. *J. Synchrotron Radiat.* **2005**, *12*, 734−738.
(23) Takamura, H.; Takahashi, N. *Solid State Ionics* **2010**, *181*, 100−103.
(24) Kamada, K.; Horiguchi, K.; Hyodo, T.; Shimizu, Y. *Cryst. Growth Des.* **2011**, *11*, 1202−1207.
(25) Munnik, F.; Benninger, F.; Mikhailov, S.; Bertsch, A.; Renaud, P.; Lorenz, H.; Gmür, M. *Microelectron. Eng.* **2003**, *67*−*68*, 96−103.
(26) Oveisi, H.; Rahighi, S.; Jiang, X.; Nemoto, Y.; Beitollahi, A.; Wakatsuki, S.; Yamauchi, Y. *Chem. Asian J.* **2010**, *5*, 1978−1983.
(27) Joint Committee on Powder Diffraction Standards (JCPDS) database: 34-0394.
(28) Bass, J. D.; Grosso, D.; Boissiere, C.; Belamie, E.; Coradin, T.; Sanchez, C. *Chem. Mater.* **2007**, *19*, 4349−4356.
(29) McBride, J. R.; Hass, K. C.; Poindexter, B. D.; Weber, W. H. J. *Appl. Phys.* **1994**, *76*, 2435−41.
(30) Bersani, D.; Antonioli, G.; Lottici, P. P.; Lopez, T. *J. Non-Cryst. Solids* **1998**, *232*−*234*, 175−181.
(31) Zhang, Q. C.; Yu, Z. H.; Li, G.; Ye, Q. M.; Lin, J. H. *J. Alloys Compd .* **2009**, *84*, 477−481.
(32) Malfatti, L.; Kidchob, T.; Aiello, D.; Aiello, R.; Testa, F.; Innocenzi, P. *J. Phys. Chem. C* **2008**, *112*, 16225−16230.
(33) Ghazzal, M. N.; Kebaili, H.; Joseph, M.; Debecker, D. P.; Eloy, P.; De Coninck, J.; Gaigneaux, E. M. *Appl. Catal. B* **2012**, *115*− *116*, 276−284.
(34) Zholobak, N. M.; Ivanov, V. K.; Shcherbakov, A. B.; Shaporev, A. S.; Polezhaeva, O. S.; Baranchikov, A. Ye.; Spivak, N. Ya.; Tretyakov Yu., D. *J. Photochem. Photobiol. B* **2011**, *102*, 32−38.
(35) X-Ray mass attenuation and mass energy-absorption coefficients of Cerium, Silicon and Titanium elements can be found at the following link: http://www.nist.gov/pml/data/xraycoef/index.cfm. (Accessed March 22, 2013).